In vivo QSM in early-stage Alzheimer's disease reveals magnetostatic alterations in the basal ganglia and beyond

Julio Acosta-Cabronero[1], Guy B Williams[2], Arturo Cardenas-Blanco[1], and Peter J Nestor[1]

[1]Brainplasticity & Neurodegeneration, German Center for Neurodegenerative Diseases (DZNE), Magdeburg, Saxony-Anhalt, Germany, [2]Wolfson Brain Imaging Centre, University of Cambridge, Cambridge, Cambridgeshire, United Kingdom

Introduction. Studying brain iron in Alzheimer's disease (AD) is particularly relevant because iron overload is a well-known feature[1]; it is thought that in neurodegenerative diseases, iron homeostasis is seriously disrupted causing iron levels to increase[2]. Biological iron, however, is multi-faceted and as such, it might hold a number of roles in neurodegeneration: iron is known to be a component of neuritic plaques[1] and neurofibrillary tangles[3], and it has been suggested that an elevated iron milieu might constitute ideal proliferation and perpetuation environments for β-amyloid aggregation and neurotoxicity[4, 5]. The ability to accurately measure iron levels *in vivo*, therefore, may offer important mechanistic insights to help unravel the sequence of events that leads to neurodegeneration. If regional changes in iron concentration in the AD brain were found to be sufficiently robust, *in vivo* measurement could even offer a diagnostic tool. **Methods.** *Subjects.* N=8 patients (age: 72±6; MMSE: 22±4) with early-stage probable AD according to NINCDS-ADRDA criteria and N=8 matched controls (age: 70±5) were recruited. *SWI.* Experiments were performed on a Siemens Trio 3T system with a 12-channel TIM head-coil using a fully flow-compensated FLASH sequence: TR/TE/α=35ms/20ms/17°; matrix, 256×240; 72 (+16 for oversampling) axial slices with voxel resolution of 1×1×2 mm^3; the total scan time was 7' (GRAPPA=2). *QSM postprocessing.* Brain masks were derived from the magnitude image using BET2 (f=0.2) with further erosion by spatial convolution with a 6-voxels-wide cubic kernel. The brain-extracted magnitude image was then RF-bias corrected (N4-ITK) and normalised to infer a noise-weighting matrix, $\mathbf{W}$. Phases were unwrapped with a direct Laplacian method[6], from which local field inductions, $\mathbf{B}_z^{\mathbf{L}}$, were estimated applying the PDF principle[7]. An in-house implementation of the MEDI approach[8] was used for conditioning the field-forward susceptibility calculation: $\mathbf{X}_{\ell_1} = \arg\min_{\mathbf{X}} \lambda \|\mathbf{W} \circ (\mathcal{D}\mathbf{X} - \mathbf{B}_z^{\mathbf{L}})\|_2^2 + \left\|\mathbf{M}_\mathbf{g}\mathcal{G}\mathbf{X}\right\|_1$, where the action of a total-variation operation, $\mathcal{G}$, masked by $\mathbf{M}_\mathbf{g}$–a sparsifying matrix that suppresses the 30% steepest magnitude gradients–further compartmentalises the fidelity-constrained solution; λ is the regularisation parameter (10 values were used, $200 < \lambda < 10000$) and $\mathcal{D}$ is the magnetic dipole convolution operator. Regularised solutions were finally normalised to a posterior ventricular region. *Structural MRI.* 3D MPRAGE volumes were also acquired–to resolve independently the underlying anatomy–with TR/TE/TI/α=2300ms/2.86ms/900ms/9°, 192×192×144 matrix and 1.25×1.25×1.25 mm^3 voxel size; scan time was 7'23''. Rigid (SWI magnitude to MPRAGE) and non-linear (MPRAGE to MNI152) coregistrations were performed using SPM8. In addition, deep GM structures were segmented using FSL-FIRST. *Stats.* Median magnetic susceptibility values for each ROI were cross-sectionally compared (AD patients versus controls) using Mann–Whitney *U* tests. For whole-brain analysis, spatially-normalised QSM reconstructions were smoothed with an 8-mm isotropic FWHM Gaussian kernel prior to FSL-randomise testing (12,870 permutations) with TFCE enabled. Results were shown at TFCE-P<0.05 (corrected for multiple comparisons). **Results.** *Parameter selection.* The most faithful (to the measured data) solution was achieved with $\lambda = 1250$. *Regional study.* Both putamena (right slightly worse than left) were highly abnormal (AD>controls, P<0.005). The left amygdala and right caudate also showed increased magnetic susceptibilities, though the effects were less pronounced (P<0.05). *Cluster-based analysis.* QSM alterations (AD>controls) were found in GM and WM tissue (see figure), specifically in the putamen bilaterally, in the left amygdala and in posterior cerebral areas. The most intense clusters were found–with relative confluence–in temporo-parietal WM and–more scattered–in posterior parietal and occipital regions. Furthermore, widespread clusters of abnormality were also found in occipito-parietal and temporo-parietal GM and WM regions. The reverse contrast did not yield any significant cluster at the present threshold level. **Discussion.** This study offers a proof of concept of QSM's strong potential to yield new insights in degenerative brain diseases such as AD. The most striking deep GM feature is a marked increase in magnetic susceptibility in the putamen. The caudate nucleus and the amygdala showed similar behaviours though differences were less statistically prominent. Ferritin is found in abnormally high concentrations in the AD basal ganglia, offering a precedent to the present results. Furthermore, recent evidence from the Dominantly Inherited Alzheimer Network (DIAN) suggests that the basal ganglia are the earliest and most intense accumulators of β-amyloid in those genetically predisposed to develop AD in the future[9]. Previous *in vivo* MRI experiments also detected abnormalities in the AD basal ganglia[10, 11], confirming that the present methodology is ready for larger scale clinical studies. The voxel-based results represent the first whole brain assessment of this kind in AD and, again, highlight the magnetic susceptibility alterations identified in the striatum by the ROI analysis. Group sizes are small, however, thus the remaining statistical effects identified beyond deep GM need to be interpreted with a little caution until replicated. Nevertheless, it is reassuring that: the whole-brain analysis could identify the striatal lesion observed by ROI extraction; that the reverse contrast (controls>AD) was completely negative; and that certain blobs appeared to be following anatomical boundaries (e.g. y=-35mm) – they all argue that the results are not spurious. It is interesting that the most extensive and significant changes were found in the posterior temporo-parietal WM, which has the greatest predilection for lobar haemorrhage and microbleeds leading to the possibility that QSM may be detecting signals related to amyloid angiopathy. Such speculation, of course, will need confirmation in future clinical studies. In contrast to WM, little convincing evidence was found for changes in the cortical ribbon though this, too, should be explored further in larger studies.

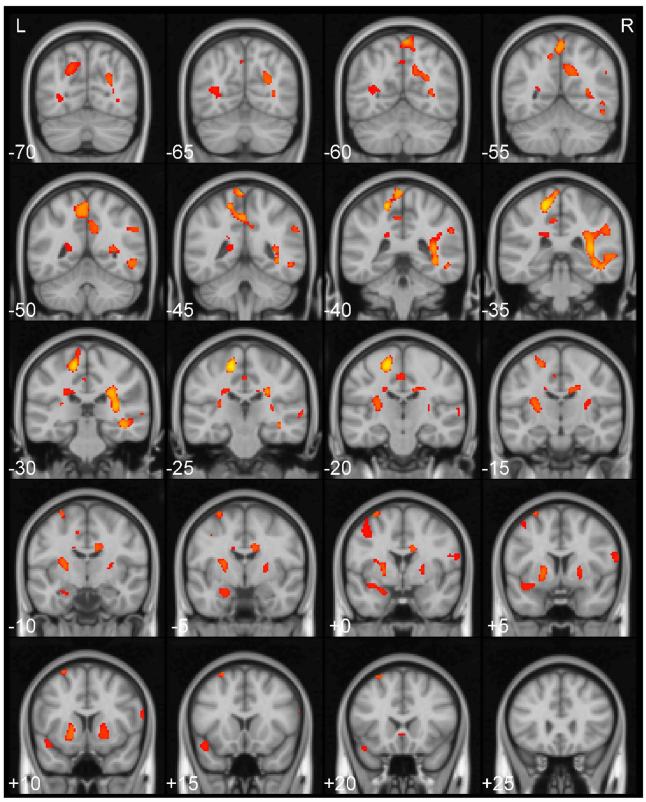

References.

1. Connor JR, Menzies SL, St Martin SM, Mufson EJ. A histochemical study of iron, transferrin, and ferritin in Alzheimer's diseased brains. *Journal of neuroscience research* 1992; 31(1): 75-83. **2.** Ke Y, Ming Qian Z. Iron misregulation in the brain: a primary cause of neurodegenerative disorders. *Lancet neurology* 2003; 2(4): 246-53. **3.** Good PF, Perl DP, Bierer LM, Schmeidler J. Selective accumulation of aluminum and iron in the neurofibrillary tangles of Alzheimer's disease: a laser microprobe (LAMMA) study. *Ann Neurol* 1992; 31(3): 286-92. **4.** Schubert D, Chevion M. The role of iron in beta amyloid toxicity. *Biochemical and biophysical research communications* 1995; 216(2): 702-7. **5.** Leskovjan AC, Kretlow A, Lanzirotti A, Barrea R, Vogt S, Miller LM. Increased brain iron coincides with early plaque formation in a mouse model of Alzheimer's disease. *Neuroimage* 2011; 55(1): 32-8. **6.** Schofield MA, Zhu Y. Fast phase unwrapping algorithm for interferometric applications. *Optics letters* 2003; 28(14): 1194-6. **7.** Liu T, Khalidov I, de Rochefort L, et al. A novel background field removal method for MRI using projection onto dipole fields (PDF). *NMR in biomedicine* 2011; 24(9): 1129-36. **8.** Liu T, Liu J, de Rochefort L, et al. Morphology enabled dipole inversion (MEDI) from a single-angle acquisition: comparison with COSMOS in human brain imaging. *Magn Reson Med* 2011; 66(3): 777-83. **9.** Bateman RJ, Xiong C, Benzinger TL, et al. Clinical and biomarker changes in dominantly inherited Alzheimer's disease. *The New England journal of medicine* 2012; 367(9): 795-804. **10.** Bartzokis G, Sultzer D, Cummings J, et al. In vivo evaluation of brain iron in Alzheimer disease using magnetic resonance imaging. *Archives of general psychiatry* 2000; 57(1): 47-53. **11.** Kirsch W, McAuley G, Holshouser B, et al. Serial susceptibility weighted MRI measures brain iron and microbleeds in dementia. *J Alzheimers Dis* 2009; 17(3): 599-609.